Nuclear Materials and Energy 12 (2017) 124–132

Contents lists available at ScienceDirect

Nuclear Materials and Energy

journal homepage: www.elsevier.com/locate/nme

A comprehensive study on impurity behavior in LHD long pulse discharges

Y. Nakamura[a,b,*], N. Tamura[a], M. Kobayashi[a,b], S. Yoshimura[a], C. Suzuki[a], M. Yoshinuma[a,b], M. Goto[a,b], G. Motojima[a,b], K. Nagaoka[a], K. Tanaka[a], R. Sakamoto[a,b], B.J. Peterson[a,b], K. Ida[a,b], M. Osakabe[a,b], T. Morisaki[a,b], the LHD Experiment Group

[a] National Institute for Fusion Science, National Institutes of Natural Sciences, Toki 509-5292, Japan
[b] SOKENDAI (Graduate School for Advanced Studies), Toki 509–5292, Japan

ARTICLE INFO

Article history:
Received 28 June 2016
Revised 14 October 2016
Accepted 12 November 2016
Available online 28 November 2016

Keywords:
Long pulse discharge
Impurity accumulation window
Radial electric filed
Impurity screening
Turbulent impurity transport

ABSTRACT

Impurity behavior is studied in a variety of LHD (Large Helical Device) long pulse discharges, i.e. standard hydrogen plasmas, super dense core plasmas, helium plasmas with ICH (Ion Cyclotron Frequency Heating), multi-species plasmas mixed with H and He. Density scan experiments show a specific density range of impurity accumulation for only hydrogen discharges. Strong suppression of impurity accumulative behavior is observed in high temperature plasmas with high power heating. The main contributions to impurity transport are extracted by a comprehensive study on impurity behavior, i.e. investigating the critical conditions for impurity accumulation and the parameter dependences. It is found that the impurity behavior is determined by three dominant contributions, i.e. neoclassical transport mainly depending on radial electric field, turbulent transport increasing with heating power and impurity screening at high edge collisionality in the ergodic layer. The mapping of impurity behavior on n-T (electron density and temperature) space at the plasma edge shows a clear indication of the domain without impurity accumulation and provides operation scenarios to build up fusion-relevant plasmas.

1. Introduction

Understanding impurity transport is one of the major tasks in present fusion research. Impurities in the plasma core enhance radiation losses and plasma dilution with deleterious consequences for fusion reactivity, and an uncontrolled impurity accumulation may even terminate the discharge. Recently, the challenges of using the high-Z plasma facing material W have been encountered in fusion devices such as ASDEX and JET [1]. The feasibility of the use of tungsten in divertor tokamaks has been intensively discussed for designing next generation fusion devices such as ITER and DEMO. The same issue is of course of relevance to helical devices. In particular, impurity handling in large superconducting heliotron/stellarator devices such as LHD [2] and W7-X [3], which should demonstrate quasi-stationary plasma operation, is an important subject [4,5].

LHD long pulse discharges with NBI heating showed impurity accumulative behavior on a long time scale (several seconds) for high-Z impurities such as Fe, which come from the plasma facing components. The intrinsic impurities were accumulated in a specific range of impurity collision frequency (impurity accumulation window), which was around the transition from the plateau regime to the Pfirsch–Schlüter (PS) regime [6,7]. Impurity transport study by using active impurity pellet injection indicated a long impurity confinement time [8]. Such an impurity behavior was also observed in other helical devices and a better understanding of impurity transport was obtained from the inter-machine comparison [9]. Theoretical predictions based on neoclassical transport theory for non-axisymmetric configurations underline the importance of radial electric field. In the standard case with negative radial electric field, the so-called ion-root regime, high-Z impurities are drawn toward the center. Only in the low-density regime, it is possible to establish the electron root with positive radial electric field, which flushes out impurities. On the other hand, impurity transport studies in the scrape-off-layer (SOL) region demonstrated a favorable impact on the impurity screening, i.e. the screening of impurity influx from the divertor plates [10,11]. Impurity transport simulations indicated a clear physical picture of impurity screening in the SOL [12]. The cross-field heat conduction governs the

* Corresponding author.
E-mail address: nakamura.yukio@LHD.nifs.ac.jp (Y. Nakamura).

http://dx.doi.org/10.1016/j.nme.2016.11.005

ion energy transport across the islands under high density, low temperature conditions. The friction force dominates over the ion thermal force, dragging impurities outwards. Turbulent transport is another important contribution to impurity transport and might gain increasing importance in fusion-relevant plasmas at high temperatures, but there is no clear evidence in experimental observation and also in theoretical analysis including simulation studies for non-axisymmetric configurations.

In order to predict impurity behavior in fusion-relevant plasmas, it is very important to extend the operational regime to high temperatures and high densities with high power heating and to explore favorable scenarios capable of preventing impurity accumulation. Recently, high NBI heating power more than 10 MW is available to long pulse operation and a variety of discharges with hydrogen plasmas, super dense core (SDC) plasmas and helium plasmas have been carried out in LHD. In this paper, impurity behavior is investigated in these discharges and a comprehensive understanding of impurity behavior in LHD long pulse discharges is presented. First of all, experimental observations are described for each discharge and some kind of parameter dependences of impurity behavior are indicated. For understanding the main contributions to impurity transport, the impurity screening effect in the ergodic layer, the role of radial electric field and the impact of turbulent transport in the core plasma are discussed. Finally, the mapping of impurity behavior on plasma parameter (n-T) space at the plasma edge is presented and operation scenarios for steady-state discharges in LHD are discussed.

2. Experimental observation on impurity behavior

LHD is a large superconducting magnetic confinement device, which employs a heliotron configuration with a pair of l/m = 2/10 helical windings [13]. A confining magnetic field of up to 2.9 T is provided in steady state by means of the full set of superconducting coils. The magnetic axis without plasma can be adjusted in the range of major radius R = 3.6–3.9 m and it is one of key parameters for producing SDC plasmas. The LHD plasma has an elongated shape with a double-null structure and the average plasma radius is about 0.6 m. Long pulse discharges can be produced by only injecting the heating power of ECH, ICH and NBI and the plasma density is controlled by gas puffing and pellet injection.

2.1. Standard hydrogen plasma with gas puffing

First of all, the distinctive features of impurity behavior in standard hydrogen discharges with the magnetic axis of R = 3.6 m are described here. Fig. 1 shows a typical long pulse hydrogen discharge with impurity accumulation. The line averaged electron density is controlled with hydrogen gas puffing during the discharge to keep a constant density of 4.5×10^{19} m^{-3}. The radiation power density in the plasma center ($\rho = 0$) increases with time though there is no big change in the radiation in the peripheral region ($\rho = 0.945$). The impurity line emission (Fe XXIII) brightens in the plasma core and the central carbon density n_C also increases remarkably with time. Fig. 2 shows the radial profiles of electron temperature, electron density, radiated power density and carbon density. The electron temperature and density profiles have a peaked shape and a flat one, respectively, and they keep nearly the same shapes during the discharge. In contrast, a remarkable peaking is observed in the radiation and the carbon density profiles, which are measured by foil bolometer arrays and charge exchange spectroscopy (CXS), respectively.

Density scan experiments in standard hydrogen discharges with gas puffing reveal the impurity accumulation window as shown in Fig. 3. In this case, the hydrogen discharges are conducted with the NBI heating power of 6.7 MW at various plasma densities in the

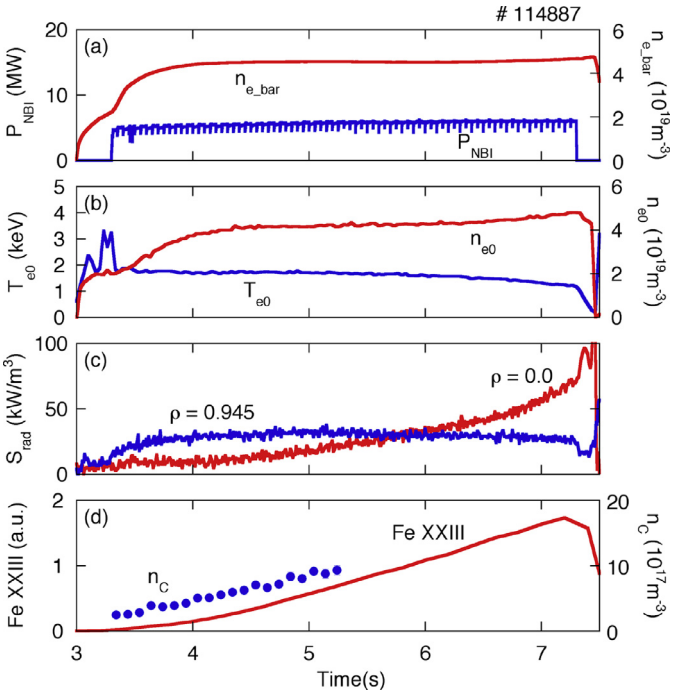

Fig. 1. Typical long pulse discharge with impurity accumulation. Time evolutions of (a) heating power of neutral beam injection and averaged electron density, (b) central electron temperature and density, (c) radiated power densities in the center and the peripheral region, (d) impurity line intensity and central carbon density are indicated.

magnetic configuration with R = 3.6 m. The relative strength of impurity accumulation is estimated by the increasing rate of radiated power in the core plasma (dS_{rad} /dt ($\rho = 0$)). As found previously, no impurity accumulation occurs in the low-density operational regime and the remarkable increase of core radiation appears with increasing density. The increasing rate of core radiation abruptly goes down and no impurity accumulation is observed in the high-density operational regime. The density range of the impurity accumulation window depends on the plasma heating power and shifts to the high density side with increasing heating power. High temperature hydrogen plasmas with the heating power of more than 10 MW reveal a new aspect of impurity behavior and the accumulation window vanishes, as described in Section 2.5.

2.2. Super dense core (SDC) plasma with pellet injection

LHD can produce SDC plasmas ($n_{e0} = 3 \sim 5 \times 10^{20}$ m^{-3}) [14,15] and recently a quasi-steady state discharge with SDC plasma [16] in the magnetic configuration R = 3.75 m has been demonstrated over 4 s by repetitive pellet injections as shown in Fig. 4. The sequential pellet injection drives the formation of a strongly peaked density profile as shown in Fig. 5(a). The density profile becomes remarkably peaked until 4.7 s. Then the central density (n_e ($\rho = 0$)) decreases and the edge density (n_e ($\rho = 1$)) increases with time. This is due to edge particle recycling, which results in the decrease of edge density by strong wall pumping in the early stage of the discharge and the gradual increase with time by reducing the capability of wall pumping. The radiation intensity is measured with bolometer arrays of absolute extreme ultraviolet photodiodes (AXUVD) [17] and the radiation signals are integrated along each chord line. A remarkable increase of radiation at the central chord is observed in the early stage of the discharge. The radiation profiles are estimated by reconstructing the two-dimensional distribution of local radiation and by superimposing each magnetic flux surface. The remarkable peaking of the radiation profile is ob-

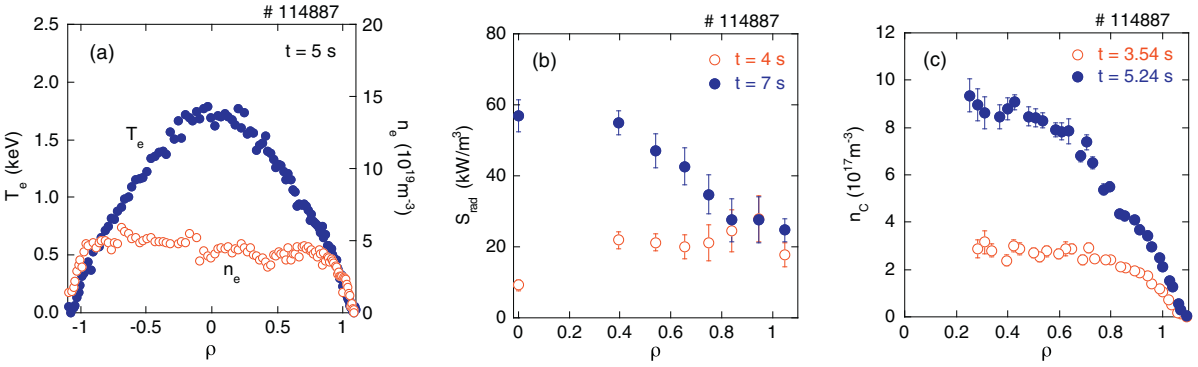

Fig. 2. Radial profiles of (a) electron temperature and density, (b) radiated power density and (c) carbon density along normalized minor radius ρ in the long pulse discharge (#114887).

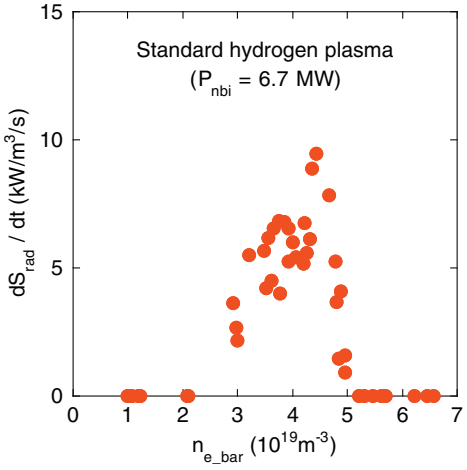

Fig. 3. Impurity accumulation window in density scan experiment with standard hydrogen plasmas. The observable indicator for impurity accumulation is the estimated increasing rate of central radiation.

served as shown in Fig. 5(c). The central radiation increases by more than three times at 4.7 s in comparison with that at 4.3 s, despite keeping the profiles of density and temperature (Fig. 5(a) and (b)). The increase of impurity line intensity (Fe XIX) in the core plasma is also observed and the global temporal behavior is the same as that of the central radiation. In this case, impurity behavior is dominated by the core impurity transport in the PS regime, where the impurity flux strongly depends on the density gradient as discussed in tokamak plasmas and the impurities are accumulated into the central region. Another important feature in these discharges is that the peaking of radiation profiles slowly stops during the discharge and no radiation collapse due to impurity accumulation is observed after the saturation ($t > 4.7$ s). This saturation is correlated to the reduction of impurity influx into the core plasma as described later (Section 3.1).

2.3. Helium plasma with ICH minority heating

In LHD, a great deal of effort has so far been devoted to achieving a steady state operation with high performance plasma and great progress has been made in terms of discharge duration and injected energy [4,5]. The high performance plasma with ion and electron temperatures of 2 keV and an averaged electron density of 1.2×10^{19} m^{-3} has been sustained for 48 min. Long pulse discharges with ICH were usually conducted in the scheme of hydrogen minority heating and helium dominant plasmas were sustained by controlling the minority ratio ($n_H/n_{He} < 0.1$). Most of long

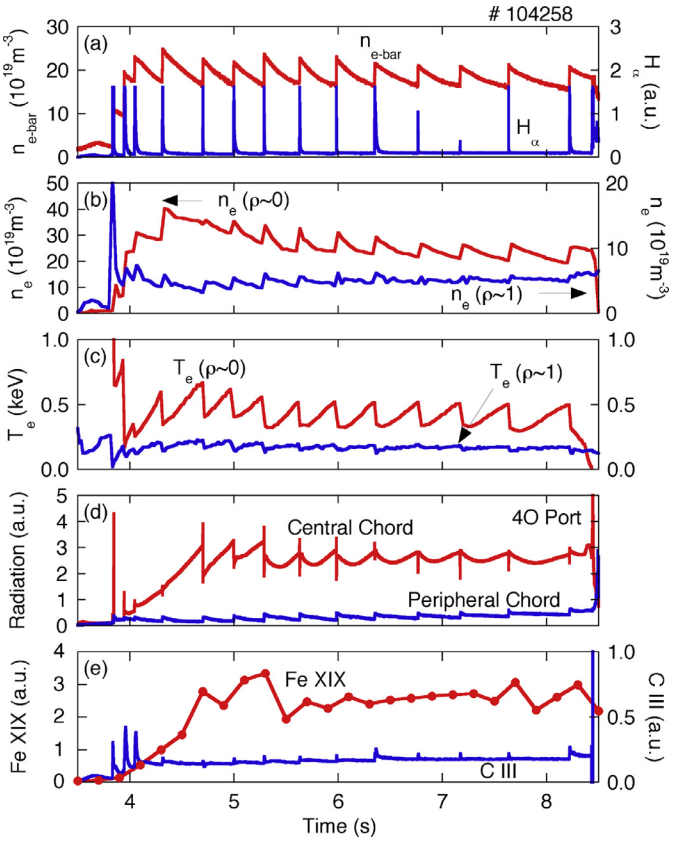

Fig. 4. Long pulse operation with super dense core (SDC) plasma by multiple pellet injection in the magnetic configuration R = 3.75 m. Time evolutions of (a) averaged electron density and Hα signal, (b) central and edge electron densities, (c) central and edge electron temperature, (d) line-integrated radiation in the central and peripheral chord, (e) impurity line intensities of Fe XIX and C III are indicated.

pulse discharges with ICH were terminated by radiation collapse due to the increase of plasma density or the penetration of impurity flakes into the plasma [18]. However, there has never been an event of long-term impurity accumulation, which is observed in hydrogen discharges. This notable result might be attributed to the difference between helium and hydrogen plasmas, i.e. the change of impurity transport due to background ions, as described later.

2.4. Multi-species plasma mixed with H and He

As described in the previous subsection, no impurity accumulation phenomenon was observed in long pulse discharges with

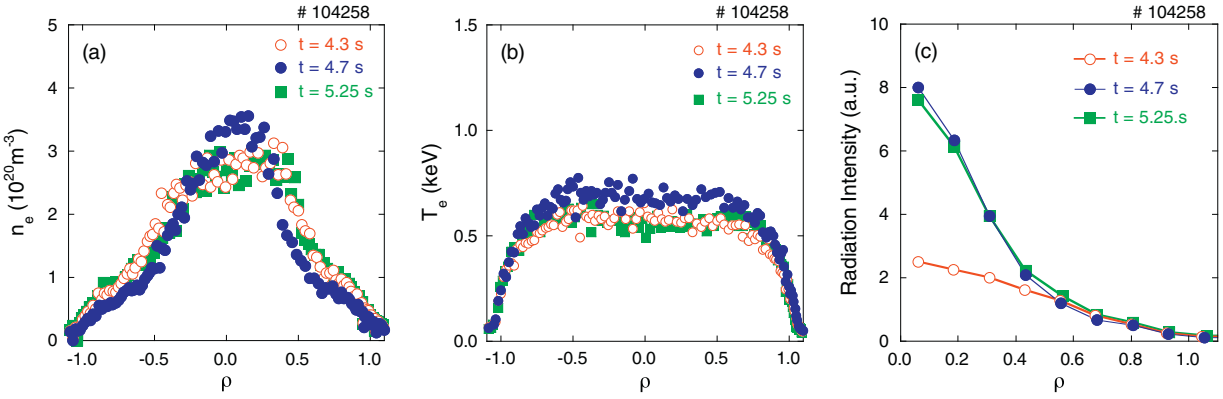

Fig. 5. Radial profiles of (a) electron density, (b) electron temperature and (c) local radiation intensity in the long pulse SDC discharge (#104258).

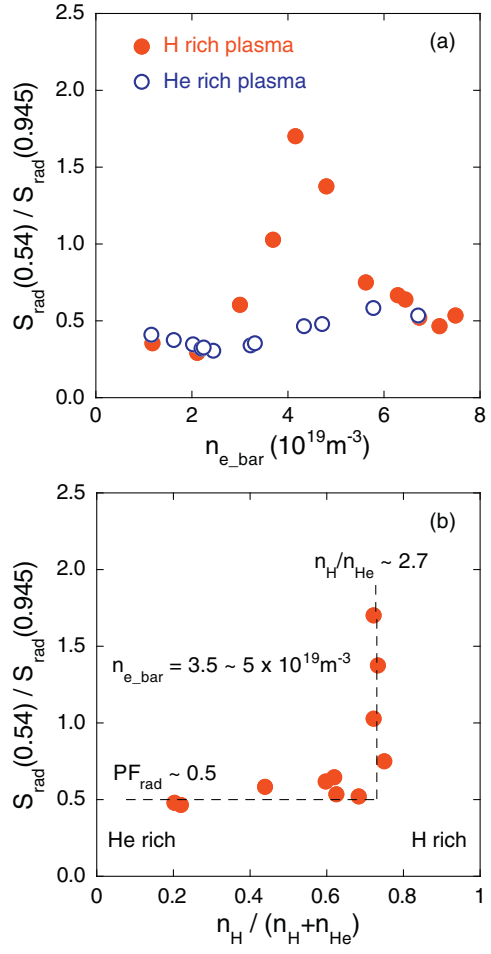

Fig. 6. Dependences of radiation peaking factor on (a) average electron density and (b) density ratio $n_H/(n_H+n_{He})$ for multi-species plasmas mixed with H and He. The peaking factor (PF_{rad}) is estimated by the ratio of core radiation ($S_{rad}(0.54)$) to edge one ($S_{rad}(0.945)$).

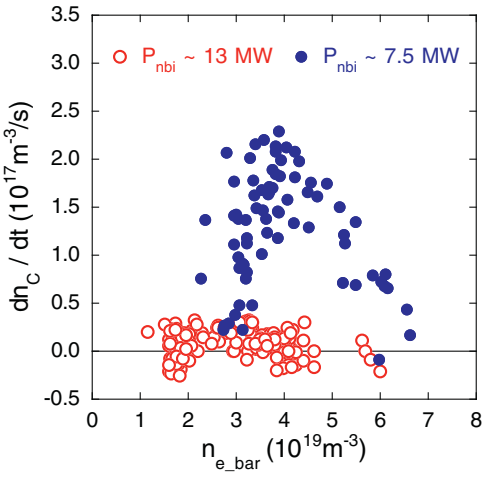

Fig. 7. Dependence of the increasing rate of core carbon density on averaged electron density for two different heating power cases ($P_{nbi}=7.5$ MW and 13 MW).

helium dominant plasmas. Therefore, impurity behavior in multi-species plasmas mixed with H and He is investigated to clarify the effect of background plasma ions on impurity transport. Density scan in long pulse discharges shows a clear difference of impurity behavior between H and He rich plasmas as shown in Fig. 6(a), where the peaking factor of the radiation profile is plotted as a function of average electron density. The impurity accumulation window is observed for H rich plasmas, while there exists no impurity accumulative behavior for He rich plasmas. Fig. 6(b) shows the dependence of the radiation peaking factor on the ratio of hydrogen ion density n_H to total ion density (n_H+n_{He}) in the discharges with $n_{e\_bar}=3.5\sim5\times10^{19}$ m^{-3}. Spectroscopic measurements with the line emission of neutral hydrogen (HI) and ionized helium (HeII) provide the average ion density ratio of hydrogen to helium (n_H/n_{He}) [19], which is available to estimate the density ratio in the plasma core for steady state plasmas [20]. The radiation peaking factor PF_{rad} remains constant until the density ratio n_H/n_{He} of 2.7 and then abruptly increases in a transitional manner. This drastic change depends on the particle transport of background ions, which influences the radial electric field determined by ambipolar diffusion and also the friction force by the collisions between impurities and background ions, as described in Section 3.

2.5. High temperature plasma with high power NBI heating

Recently, high NBI heating powers ($P_{nbi}>10$ MW, $t_d\sim5$ s) are available for steady-state discharges and it enables us to study impurity behavior in high temperature plasmas. In these discharges, it is found that the impurity accumulative behavior is dramatically suppressed with higher NBI heating power. Fig. 7 shows the dependence of the increasing rate of core carbon density on line-averaged electron density for two different heating power cases. In the case of low power heating ($P_{nbi}=7.5$ MW), the density window for impurity accumulation is found in the carbon density mea-

surement as observed before in radiation measurements (Fig. 3). However, the impurity accumulation window almost vanishes in the discharges with high power heating (P_{nbi} = 13 MW). The high temperature plasmas in the impurity accumulation window have a large negative radial electric field in the edge region and it is expected that the impurities are driven into the core plasma. The impurity screening in the ergodic layer depends on the temperature and density in the SOL, but the plasma parameters do not satisfy the criterion for impurity screening in the ergodic layer. A new contribution to impurity transport is required for understanding the result in high temperature plasmas and discussed in Section 3.2.3.

3. Comprehensive understanding of impurity behavior

The impurity evolution in plasmas depends on transport processes in the three plasma regions: (a) the plasma-surface interaction zone, (b) the scrape-off layer (SOL) and (c) the plasma confinement region. In steady state discharges, impurity influx due to the sputtering of plasma facing components remains almost constant because there is no big change in the plasma parameters in the SOL during the discharge. Therefore, the screening processes in the SOL and the confinement properties of the core plasma are comprehensively studied using experimental observations in a variety of long pulse discharges.

3.1. Impurity influx screening in the ergodic layer

Particle and energy transport in the SOL have been extensively investigated in helical systems as well as in tokamaks. Recent studies of edge impurity transport with the EMC3/EIRENE code indicated a clear physical picture of impurity screening in the SOL, which is a unique feature in helical devices [12]. The balance between friction and ion thermal forces governs the edge impurity transport and the impurity influx into the core is strongly reduced in the friction-dominated regime. This reduction is caused by a strong suppression of the thermal force due to the enhancement of cross-field heat conduction through the magnetic islands. Therefore, the ratio of the parallel ($Q_{//D}$) to the perpendicular heat flux ($Q_{\perp D}$) can be regarded as a key parameter for the impurity screening effect [21]:

$$\frac{Q_{\|D}}{Q_{\perp D}} = \frac{\Theta^2 k_{i0} T_i^{5/2}}{\chi_{i\perp} n_i} = \xi_i \qquad (1)$$

The field-line pitch Θ plays an important role in the transport process. The contribution of cross-field transport remarkably increases only for helical systems with Θ = 0.0001 ~ 0.001, which is extremely different from Θ ~ 0.1 for tokamaks. The impurity screening in the ergodic layer can be expected when the cross-field heat conduction becomes even more dominant under the condition $\xi_i < 1$ [22]. This geometrical 3D effect is under investigation with the multi-machine comparison [23].

In the standard hydrogen discharges with gas puffing (R = 3.6 m), the impurity accumulation is strongly suppressed in the high density region (Fig. 3). The experimental database of impurity behavior has been constructed by scanning the plasma density in long pulse discharges with NBI heating power between 1 MW and 9.5 MW. The experimental study of the critical condition on impurity screening indicated an empirical scaling based on the above impurity transport theory, i.e. $\xi_i \sim 0.11$ [21]. Here, it is important to investigate whether or not the scaling can be applied to other discharges such as to the SDC plasma or to the He rich plasma. Fig. 8 shows a mapping of the SDC plasmas and the standard hydrogen plasmas on the two-dimensional space of the electron density and temperature at the last closed flux surface (LCFS). In this case, both SDC and standard hydrogen plasmas

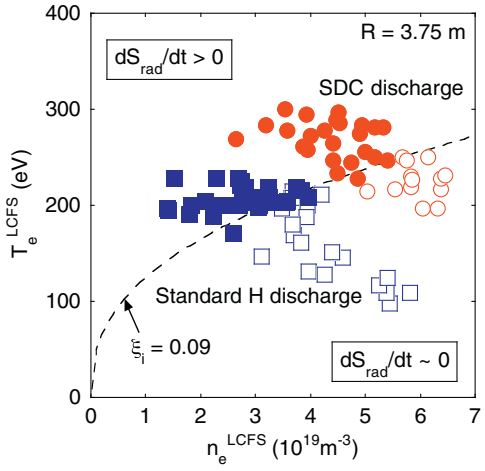

Fig. 8. Mapping of SDC plasmas and standard hydrogen plasmas on n-T space at the plasma edge. Both SDC and standard hydrogen plasmas are produced in the magnetic configuration R = 3.75 m. The closed and open symbols indicate the plasmas with and without impurity accumulation at each time in the discharges (e.g. # 104258 in Fig. 4), respectively. The dashed line is fitted by the curve of constant ξ_i parameter.

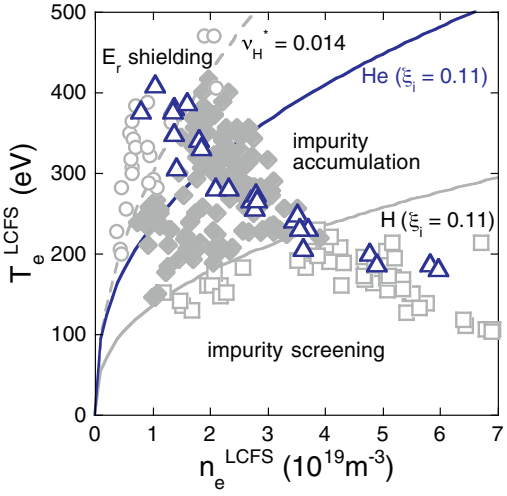

Fig. 9. Mapping of He rich plasmas and standard hydrogen plasmas on n-T space at the plasma edge. The light gray symbols and open triangles indicate hydrogen plasmas and He rich plasmas, respectively. The solid and dashed lines of light gray indicate the empirical scaling on impurity screening for hydrogen plasmas [21]. The bold solid line is estimated for pure helium plasmas by using the same ξ_i parameter for hydrogen plasmas.

are produced in the magnetic configuration with R = 3.75 m. The closed symbols indicate the plasmas with impurity accumulation ($dS_{rad}/dt > 0$) and the open symbols the plasmas without impurity accumulation ($dS_{rad}/dt \sim 0$). The critical condition can be estimated by the curve of constant parameter ξ_i (see Eq. (1)), which is expressed as $T = C_H\, n^{0.4}$ with a specific constant value of C_H given by $(\chi_{i\perp}\xi_i/\Theta^2\kappa_{i0})^{0.4}$. The curve with the constant $C_H \sim 125$ makes a clear separation between impurity accumulation and impurity screening regions. Assuming that the perpendicular thermal diffusivity $\chi_{i\perp} \sim 1\ m^2/s$ for LHD with $\Theta \sim 10^{-4}$, the constant C_H (= 125) corresponds to the ratio of the parallel to the perpendicular heat flux $\xi_i \sim 0.09$, which is almost the same as that ($\xi_i \sim 0.11$) in the magnetic configuration with R = 3.6 m.

For He plasmas, there is a possibility of reducing the parallel heat conduction in comparison with the H plasmas because the coefficient of ion heat conductivity depends on the mass and the charge of background plasma ion ($\kappa_{i0} \propto m_i^{-1/2} Z_i^{-2}$). Fig. 9 shows a

mapping of the He rich plasmas and the previous standard hydrogen plasmas on the n-T space at the LCFS. The light gray symbols (solid or open) indicate the hydrogen plasmas and the open triangles the He rich plasmas, in which there exists no impurity accumulation over all density range. The solid line of light gray represents the empirical scaling for impurity screening for hydrogen plasmas and the solid line for pure helium plasmas, taking into account the differences in the mass and the charge in comparison with pure hydrogen plasmas. Though the impurity screening area expands to the low collisionality side for the He plasmas, it is not enough to explain the suppression of impurity accumulation in the low collisionality region. Even with that, the impurity screening at high edge collisionality is effective for all long pulse discharges.

3.2. Impurity transport in the core plasma

Impurity transport studies in the core plasma have been performed in various helical devices [8,24,25], analyzing the temporal and spatial evolution of impurity radiation in response to transient impurity sources. For this purpose, impurity ions different from the intrinsic impurities were injected into the plasma either by using a tracer-encapsulated solid pellet (TESPEL) [26] or a laser blow-off technique. The decay times of the corresponding line emission of the highest ionization states after the injection were taken as a measure of the impurity confinement time. The inter-machine comparison studies show a clear density dependence of the impurity confinement time, which increases with the plasma density and yields longer confinement times at higher density [9]. This result may be connected with neoclassical and turbulent impurity transport and the unfavorable density dependence is qualitatively in good agreement with neoclassical theory, where the ambipolar radial electric field dominates impurity transport for high Z impurities. In the tracer approximation without the interaction between impurities and background ions, the neoclassical impurity flux density in the bulk plasma can be expressed by

$$\Gamma_z = -n_z D_{11}^z \left\{ \frac{n'_z}{n_z} - \frac{ZeE_r}{T_i} + \frac{D_{12}^z}{D_{11}^z} \frac{T'_z}{T_z} \right\} \quad (2)$$

for impurity ions with the ionic charge eZ, density n_Z and the radial electric field E_r determined by the ambipolar condition [9,27]. With increasing Z, the second term inside the brackets becomes dominant in the convection terms and depends strongly on the radial electric field. Therefore, high-Z impurities are drawn toward the center by negative E_r and pushed outward by positive E_r. As a result, the impurity behavior is strongly influenced by the polarity of the radial electric field. On the other hand, there is no clear evidence of turbulent impurity transport in experimental observation and theoretical analysis including simulations. In this subsection, the role of the radial electric field in impurity behavior is investigated for a variety of long pulse discharges and some convincing indications pointing to the essential role of anomalous impurity transport are discussed for high temperature plasmas with high power NBI heating.

3.2.1. Impurity core confinement time

First of all, the impurity confinement time is investigated by using TESPEL to confirm the similarity of impurity behavior between intrinsic impurities and externally injected impurities. In the standard hydrogen discharges, the impurity confinement time increases with the collisionality and the extrinsic impurities have a very long confinement time in impurity accumulation window. The similar long confinement behavior is seen for SDC hydrogen discharges. On the other hand, in helium discharges without impurity accumulation, the injected impurities are flushed out instantaneously. For high temperature hydrogen discharges, the strong pumping out of the tracer impurity is observed as in helium discharges. Thus similar confinement behavior is observed between intrinsic and extrinsic impurities. Another important point is that the extrinsic impurities have a long confinement time even in the high density range, where the SOL impurity screening mechanism becomes active, for standard hydrogen plasmas and SDC plasmas.

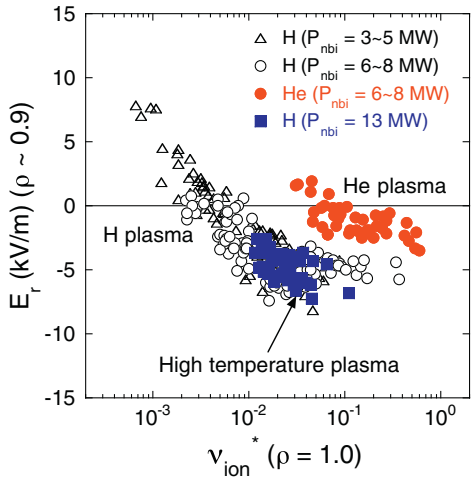

Fig. 10. Radial electric field in the plasma edge region as a function of background ion collisionality for H and He plasmas with different heating powers.

3.2.2. Role of radial electric field

E_r measurements have been carried out in a variety of LHD hydrogen plasma as with a wide range of density and magnetic axis. The dependences of E_r on density and magnetic configuration are qualitatively consistent with neoclassical theory [28]. In particular, a significant change of E_r appears in the edge plasma region. E_r in the edge region changes its sign from positive in the electron root to negative in the ion root with increasing density. Fig. 10 shows the dependence of E_r on background ion collisionality ($\nu_{ion}{}^* = \nu/(v_{th}/qR_0)$) at the LCFS ($\rho = 1.0$) for hydrogen and helium plasmas with a wide range of heating power and density. In this figure, one can see that the radial electric field at the plasma edge ($\rho \sim 0.9$) does not depend on the heating power but depends only on the ion collisionality. Therefore, the background ion collisionality can be regarded as a good predictor of E_r. Another important point is the difference between H and He plasmas in the E_r value. For helium plasmas, it is hard to enter the ion root (negative E_r) deeply even in the high collisionality region. This is due to the difference of the particle flux between H and He ion species, which strongly influences the E_r determined by the ambipolar condition ($\Sigma\ Z_a \Gamma_a{}^{na} = 0$). The helium ion flux in pure He plasmas is remarkably reduced in comparison with the hydrogen ion flux in H plasmas and the radial electric field does not reach a large negative value even in the high density region [29].

LHD has a large flexibility in changing the ambipolar radial electric field E_r by controlling the effective ripple and the magnetic topology and the impact of E_r on impurity transport was studied in different magnetic configurations [21]. Both the impurity accumulation window and E_r points were shifted to the high collisionality side with a shifting of the magnetic axis outward and the critical condition for impurity accumulation was in good agreement with the change of E_r. Moreover, recent simultaneous measurements of both key parameters (E_r and core radiation) indicate a direct casual relationship between E_r and impurity behavior in the low collisionality region as shown in Fig. 11. In this figure, no discharge exists with a density of more than $5 \times 10^{19}\ m^{-3}$, thereby eliminating the impurity screening effect in the high collisionality region.

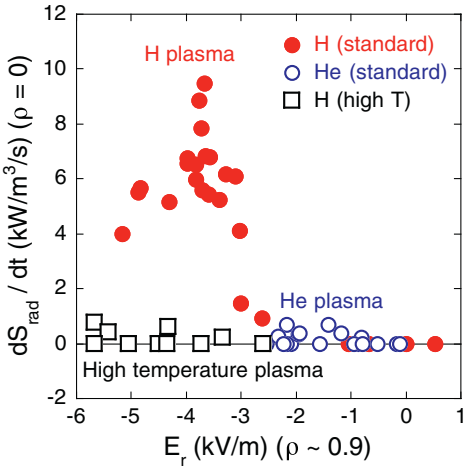

Fig. 11. Relationship between the radial electric filed at the plasma edge and the increasing rate of core radiation in standard H, He and high temperature plasmas.

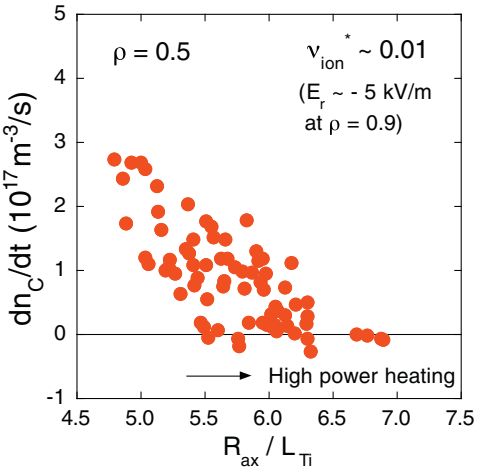

Fig. 12. Correlation between the increasing rate of carbon density and ion temperature gradient in hydrogen plasmas with the constant ion collisionality ($\nu_{ion}^* \sim 0.01$) at $\rho = 0.5$. The ion collisionality corresponds to that of 0.025 at $\rho = 1.0$ and $E_r \sim -5$ kV/m at the plasma edge ($\rho \sim 0.9$).

In the standard hydrogen discharges, when E_r decreases with increasing density, the observable indicator of impurity accumulation (dS_{rad}/dt) abruptly increases at a specific value of $E_r \sim -3$ kV/m. The impurity accumulative behavior is always observed in the ion root regime with the large negative E_r value (<-3 kV/m). For helium discharges, E_r cannot reach the specific value even at the density of around 5×10^{19} m^{-3} and no impurity accumulation is observed ($dS_{rad}/dt \sim 0$). From both results, it seems that the impurity transport in the plasma core is attributed to the radial electric field for H and He standard discharges. In SDC hydrogen discharges ($R = 3.75$ m), it is hard to discuss the relationship between E_r and impurity accumulation because there is no database on the radial electric field. However, the E_r can be expected to be a large negative value from the plasma parameters (collisionality) in the edge region and therefore the intrinsic impurities can enter into the plasma core. The core plasma with very high density is in the PS regime and the impurities may be drawn toward the center due to a steep density gradient and a flat temperature profile, which is predicted by neoclassical theory in tokamak plasmas [30]. At last, any clear indication of relevance between E_r and impurity behavior cannot be found for high temperature plasmas with high power heating. There is no impurity accumulation even in high temperature plasmas with large negative E_r values, which is very different from the impurity behavior in standard hydrogen plasmas. This suggests that there exists some kind of outward convection driven by turbulence as discussed in the next subsection.

3.2.3. Impact of turbulent transport

In tokamaks, impurity transport studies have been investigated with neoclassical transport theory and temperature-screening effect in improved plasmas with high ion temperature is well known [31]. On the other hand, recent studies of turbulent impurity transport are starting to demonstrate promising qualitative and quantitative agreement between impurity measurements and gyrokinetic turbulence simulations. However, the screening effect is not expected in helical system except for high collisionality regime [9] and turbulent impurity transport is very limited in experiments and theoretical analysis for helical devices. In our case, it is also difficult to obtain direct experimental evidence of turbulent transport. Therefore, some convincing indications pointing to the essential role of anomalous impurity transport are described.

First of all, in the experiment with impurity pellet injection, anomalous coefficients originating from turbulent transport processes have to be used to fit the experimental results. The transport simulations reveal diffusion coefficients being one order of magnitude enhanced over neoclassical levels for high temperature plasmas [32]. Secondly, as described in the previous subsection, for standard hydrogen discharges with $P_{nbi} < 10$ MW, impurity transport in the core plasma is dominated by the radial electric field, which is predicted by neoclassical theory for high Z impurities. To keep the E_r contribution constant, specific discharges with constant ion collisionality are selected from those with various heating powers, because the ion collisionality is a good predictor of E_r. The turbulent contribution to impurity transport is extracted by investigating the dependence of the impurity pinch on the ion temperature gradient, which can drive turbulence (ITG mode). Fig. 12 shows the correlation between the increasing rate of carbon density and the ion temperature gradient for hydrogen plasmas with the constant ion collisionality ($\nu_{ion}^* \sim 0.01$) at $\rho = 0.5$. The ion collisionality corresponds to that of around 0.025 at $\rho = 1.0$, where impurity accumulative behavior remarkably appears as shown in Fig 9. In this case, the strength of the impurity pinch is calculated by the time derivative of the carbon density at the mid-radius ($\rho = 0.5$). At the same radial position, the normalized logarithmic ion temperature gradient $R_{ax}/L_{Ti} = -(R_{ax}/T_i)dT_i/dr$ is estimated from the ion temperature profile measured by CXS. One can see a significant decreasing trend of the impurity pinch when the temperature gradient is increased with the heating power. Consequently, there is no observation of impurity accumulative behavior in high temperature plasmas with high power heating ($P_{nbi} = 13$ MW). In this database, as a matter of course, there is no sensitivity to the radial electric field, which depends on only ion collisionality ($E_r \sim -5$ kV/m at $\rho = 0.9$ for $\nu_{ion}^* \sim 0.01$). Therefore, this trend cannot be explained by neoclassical impurity transport. Another important feature is seen in the carbon density profile for high temperature plasmas as shown in Fig. 13. The carbon density profile becomes hollow with decreasing the plasma density, thereby observing a strong hollow profile of carbon, the so-called impurity hole in high ion temperature mode [33–35]. Although the impurity hole is observed as a transient phenomenon in high T_i mode, such a strong hollow carbon profile is sustained for long time during the standard hydrogen discharge with high power heating. The hollowness of the carbon profile becomes stronger with decreasing background ion collisionality as shown in Fig. 14, where the normalized logarithmic carbon density gradient $R_{ax}/L_{nc} = -(R_{ax}/n_c)dn_c/dr$ is plotted as a function of ion collisionality. In general, the radial electric field increases with decreasing ion collisionality and becomes positive to drive the impurities outward.

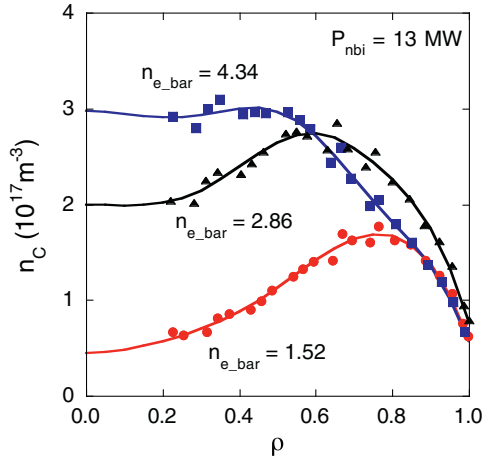

Fig. 13. Carbon density profiles in high temperature plasmas with different average densities. Each carbon density profile is maintained during the discharge.

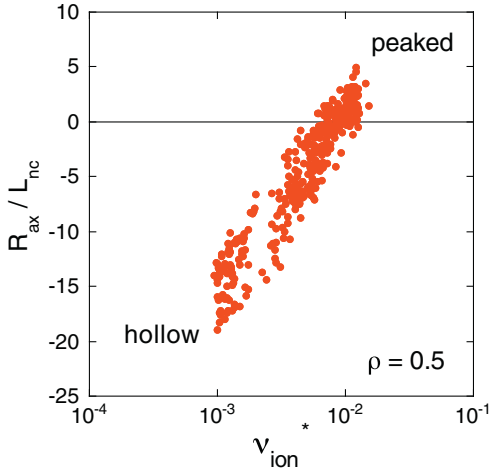

Fig. 14. Correlation between carbon density profile and ion collisionality. The vertical axis indicates the normalized logarithmic carbon density gradient (R_{ax}/L_{nc}) at the mid-radius.

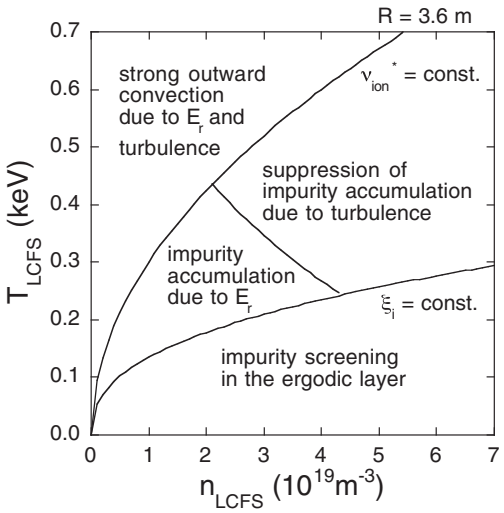

Fig. 15. Classification of impurity behavior on n-T space at the plasma edge in the operational regime on LHD with R = 3.6 m. The n-T diagram is made for standard hydrogen plasmas with flat density and peaked temperature profiles. The dominant contribution to impurity transport is indicated in each domain. The solid lines are based on the empirical scaling determined by the mapping of various discharges.

However, the radial electric fields in the core region can be evaluated to be negative for high temperature plasmas, because the E_r is a monotonic function of minor radius in LHD [36] and has a negative value at the plasma edge (Fig. 10). Therefore, the strong outward convection at around the mid-radius cannot be explained by neoclassical impurity transport alone. One of most probable candidates for anomalous impurity transport is turbulence such as the ITG mode, which can be driven in high temperature plasmas ($R_{ax}/L_{Ti} > 5$) in LHD [37]. Although turbulent impurity transport simulation is under investigation in LHD, there are some results on turbulent impurity transport for tokamak plasmas. In a reversed magnetic shear configuration, which has a negative magnetic shear as well as LHD, the curvature pinch provides the main contribution to the total convective velocity and becomes outward in turbulent transport simulation [38]. Comparison between measured boron profiles and gyrokinetic simulations indicates that thermodiffusion (ion temperature gradient) and rotodiffusion (toroidal rotation gradient) terms contribute to the outward convection in turbulent impurity transport [39,40]. These results indicate that ITG turbulence drives the impurities outward in experimental observations and simulation studies. In LHD, recent studies on impurity transport in the discharge with NBI torque input show that toroidal rotation plays an important role in the impurity transport [41]. The impurity behavior in LHD may be dominated by a combination effect of ion temperature gradient and rotation gradient terms in turbulent impurity transport. The anomalous impurity transport observed in high temperature plasmas has a good similarity with the recent results in tokamak plasmas.

3.3. Operational regime without impurity accumulation

A large number of long pulse discharges have so far been performed to explore the operational regime without impurity accumulation. The experimental database enables us to make a mapping of impurity behavior in the steady state operational regime. Fig. 15 shows a diagram for impurity behavior on the plasma parameters (n, T) at the plasma edge, which is made for standard hydrogen plasmas with gas puffing in the magnetic configuration with R = 3.6 m. In these discharges, the profile structures in density and temperature (flat density and peaked temperature) are kept for scanning the density and heating power. The degree of turbulence increases with increasing heating power (temperature gradient). The impurity behavior is basically determined by three dominant contributions to impurity transport: (a) neoclassical transport due to the radial electric field, (b) anomalous transport due to turbulence and (c) impurity screening in the ergodic layer. In the low collisionality region with low n and high T, the plasma has a large positive E_r which prevents the impurities from entering into the plasma core. The steep ion temperature gradient drives ITG turbulence, inducing the outward convection of impurity ions. As a result, extremely hollow impurity profiles are observed by a strong outward convection due to the synergetic effect of positive E_r and turbulence. On the other hand, in the high collisionality region with high n and low T, though the plasma has a large negative E_r drawing the impurities into the plasma core, the impurity screening by the friction force is effective in the SOL. Consequently, the intrinsic impurities are retained in the SOL region and no impurity accumulation is observed. The boundary conditions are determined by the constant ion collisionality and ξ_i parameter, which are empirically derived from the experimental database. In the intermediate collisionality region, the plasma is in the ion root regime with negative E_r, while turbulence increases in intensity with increasing heating power. As the E_r does not depend on the heating power and the neoclassical pinch term E_r/T_i decreases with increasing ion temperature [42], turbulent transport becomes dominant in higher

temperature plasmas, thereby resulting in the strong suppression of accumulation. Here, the boundary condition is empirically determined by the heating power, $P_{nbi} = 10$ MW, which corresponds to a power density of approximately 1 MW/m^3 in the plasma core. From this figure, it is found that the domain of impurity accumulation is restricted to the specific collisionality range and vanishes in the higher temperature region, which is a big advantage for achieving steady state operation in fusion-relevant plasmas.

4. Summary

A systematic study of impurity behavior has been performed with a variety of long pulse discharges. Some kinds of impurity accumulative behavior are observed and the intrinsic impurities such as iron and carbon are accumulated into the plasma core. Density scans in standard hydrogen discharges reveal a specific density range of impurity accumulation, i.e. an impurity accumulation window. In SDC discharges, transient impurity accumulation is observed in the initial stage of the discharge and thereafter the long-term accumulative behavior does not appear. This is caused by the change of edge density due to particle recycling. There is no observation of impurity accumulation in steady state discharges with ICH minority heating, which requires a very small density ratio of H to He ions. Multi-species plasmas mixed with H and He show a distinctive difference in impurity transport due to background ions. Although there exists no impurity accumulation window for He rich plasmas, the accumulation window appears in a transitional manner with a decreasing density ratio of He to H. High temperature plasmas with high power heating indicate the strong suppression of impurity accumulative behavior and no impurity accumulation is observed over the entire density range.

The impurity behavior is comprehensively investigated from the three points of view of impurity transport, i.e. impurity screening in the SOL, the role of E_r in neoclassical transport and the contribution of turbulence. Impurity screening due to the friction force at high edge collisionality is studied for standard hydrogen discharges and an empirical scaling on the critical condition is found. This scaling can be applied to the SDC plasmas and the multi-species plasmas mixed with H and He, and the impurity screening is effective for all discharges. In the plasma core, neoclassical impurity transport is basically dominated by E_r, which depends on the background ion collisionality. Since He plasmas do not enter in a deep ion root regime with a large negative E_r even in the high density region, the E_r contribution is significantly reduced in the impurity accumulation window. The direct correlation between E_r and core radiation also shows the importance of the E_r contribution to core impurity transport for H and He plasmas. Some convincing contributions of turbulence are observed in higher temperature plasmas. The suppression of impurity accumulative behavior increases with increasing ion temperature gradient under the constant E_r contribution. Carbon density measurements reveal a strong hollow profile in high temperature plasmas at low density and the carbon density gradient becomes stronger with decreasing ion collisionality. One of most probable candidates for anomalous impurity transport is turbulence such as the ITG mode, which drives the impurities outward for tokamak plasmas. However, further investigation into turbulent transport is required.

The impurity behavior in long pulse discharges can be classified on the n-T diagram at the plasma edge and divided into four categories: (a) impurity screening at high edge collisionality in the ergodic layer, (b) strong outward convection due to positive E_r and turbulence in the low collisionality region, (c) impurity accumulation by the dominant contribution of negative E_r, (d) turbulent transport exceeding neoclassical transport (E_r/T_i pinch term) and suppressing impurity accumulation. From this diagram, operation scenarios of steady state plasmas in LHD can be developed towards the realization of fusion-relevant plasmas.

Acknowledgments

The authors are grateful to the LHD Team for their excellent cooperation and to the device engineering group of LHD for maintaining good operating conditions. One of the authors (YN) thanks the referees for their important comments and fruitful discussions. This work is supported by the budget for the LHD project (NIFSULRR702).

References

[1] M.N.A. Beurskens, et al., Plasma Phys. Control. Fusion 55 (2013) 124043.
[2] O. Kaneko, et al., Nucl. Fusion 53 (2013) 104015.
[3] T.S. Pedersen, et al., Nucl. Fusion 55 (2015) 126001.
[4] Y. Nakamura, et al., Nucl. Fusion 46 (2006) 714.
[5] T. Mutoh, et al., Nucl. Fusion 53 (2013) 063017.
[6] Y. Nakamura, et al., Plasma Phys. Control. Fusion 44 (2002) 2121.
[7] Y. Nakamura, et al., Nucl. Fusion 43 (2003) 219.
[8] N. Tamura, et al., Plasma Phys. Control. Fusion 45 (2003) 27.
[9] R. Burhenn, et al., Nucl. Fusion 49 (2009) 065005.
[10] M. Kobayashi, et al., J. Nucl. Mater. 390-391 (2009) 325.
[11] M. Kobayashi, et al., Nucl. Fusion 53 (2013) 033011.
[12] Y. Feng, et al., Plasma Phys. Control. Fusion 53 (2011) 024009.
[13] A. Iiyoshi, et al., Nucl. Fusion 39 (1999) 1245.
[14] N. Ohyabu, et al., Phys. Rev. Lett. 97 (2006) 055002.
[15] R. Sakamoto, et al., Nucl. Fusion 49 (2009) 085002.
[16] H. Yamada, et al., Nucl. Fusion 51 (2011) 094021.
[17] B.J. Peterson, et al., Plasma Phys. Control. Fusion 45 (2003) 1167.
[18] H. Kasahara, et al., Phys. Plasma 21 (2014) 061505.
[19] M. Goto, et al., Phys. Plasma 10 (2003) 1402.
[20] K. Ida, et al., Rev. Sci. Instrum. 86 (2015) 123514.
[21] Y. Nakamura, et al., Plasma Phys. Control. Fusion 56 (2014) 075014.
[22] Y. Feng, et al., Nucl. Fusion 46 (2006) 807.
[23] M. Kobayashi, et al., Nucl. Fusion 55 (2015) 104021.
[24] R. Burhenn, et al., Fusion Sci. Technol. 46 (2004) 115.
[25] C. Hidalgo, et al., Nucl. Fusion 45 (2005) S266.
[26] S. Sudo, et al., Nucl. Fusion 52 (2012) 063012.
[27] H. Maassberg, et al., Plasma Phys. Control. Fusion 41 (1999) 1135.
[28] M. Yoshinuma, et al., Plasma Phys. Control. Fusion 46 (2004) 1021.
[29] H. Sasao, et al., J. Plasma Fusion Res. Ser. 3 (2000) 431.
[30] S.P. Hirshman, D.J. Sigmar, Nucl. Fusion 21 (1981) 1079.
[31] M.R. Wade, et al., Phys. Rev. Lett. 84 (2000) 282.
[32] S. Sudo, et al., Plasma Phys. Control. Fusion 55 (2013) 095014.
[33] M. Yoshinuma, et al., Nucl. Fusion 49 (2009) 062002.
[34] K. Ida, et al., Phys. Plasma 16 (2009) 056111.
[35] M. Yoshinuma, et al., Nucl. Fusion 55 (2015) 083017.
[36] K. Ida, et al., Nucl. Fusion 45 (2005) 391.
[37] M. Nakata, et al., Plasma Phys. Control. Fusion 58 (2016) 074008.
[38] S. Futatani, Phys. Rev. Lett. 104 (2010) 015003.
[39] C. Angioni, et al., Nucl. Fusion 51 (2011) 023006.
[40] E.J. Casson, et al., Nucl. Fusion 53 (2013) 063026.
[41] Y. Nakamura, in: 26th IAEA Fusion Energy Conference (Kyoto, Japan), 2016, p. EX/P8-4.
[42] J.L. Velasco, et al., Nucl. Fusion 57 (2017) 016016.